Taylor & Francis
Taylor & Francis Group

Fourier finite element model for prediction of thermal buckling in disc clutches and brakes

Zhuo Chen, Yun-Bo Yi, and Jiaxin Zhao

Department of Mechanical and Materials Engineering, University of Denver, Denver, Colorado, USA

ABSTRACT

Numerical analyses are performed on thermal buckling of annular rings using a reduced Fourier method. The stress stiffness matrix is derived from the geometric nonlinearity in the Green strains with a predefined circumferential wave number. The method is first validated through the commercial software Abaqus using an axisymmetric model. It is then implemented to solve more general nonaxisymmetric problems with multiple waves along the circumference. It is shown that there exists a particular wave number with which the buckling temperature reaches a minimum. This research has potential applications in automotive clutch and brake designs against thermal buckling.

Introduction

Frictional heat generation in automotive brake and clutch systems can cause excessive thermal stresses, thermoelastic instability (TEI) as well as thermal distortion or buckling [1–3]. Although the investigations on TEI have been performed by many researchers over the last decades, the interest in thermal buckling is, more recent, mainly prompted by the experimental findings in multidisc clutch applications [4]. The observed nonuniform temperature distribution along the radius can lead to a hoop stress or bending moment that exceeds the upper limit of elastic stability [5]. Unlike a straight beam or column, the axisymmetric mode or the *coning* mode in brake and clutch discs can be one of the dominant modes with the lowest buckling temperatures, in addition to the circumferential wavy modes or the so-called *potato chip* modes [6].

Timoshenko's beam theory [7] can be applied on a curved beam to derive an approximate solution for the critical buckling load in a disc ring, assuming that the beam may buckle laterally under a sufficiently large bending moment. However, the solution thus obtained is based on the classical beam model with a simplified treatment of the stress variations in the radial direction. This can lead to an inaccuracy in the solution when the radial width is comparable with the disc size. Ma [8] investigated the effects of three-dimensional geometries and different material properties on the critical buckling loads based on a set of finite element analyses using Abaqus. Later Zhao et al. [9] extended Ma's techniques by taking into account the effects of a variety of temperature profiles. It was found that the radial variation of temperature considerably affects the critical buckling load.

The commercial finite element codes such as Abaqus can handle three-dimensional thermal buckling problems using the appropriate element types [10]. Usually, only the lowest buckling modes have practical meanings, however these modes can have very close eigenvalues, especially in a 3D model. Therefore, in many situations, it is still necessary to extract a relatively large number of modes from the solution. We found that it is inconvenient to study the eigenvalue as a function of the wave number by manually sorting the solutions according to the deformation shapes. On the other hand, the

axisymmetric element library available in the software makes it possible to deal with the coning modes in the special case, when the thermal loading and the deformation shape are both circumferentially uniform and can therefore take advantage of the geometric symmetry. However it has been found that the buckling temperature of coning modes could be much higher than those of the potato chip modes. Using an axisymmetric model would be inappropriate when the deformation and thermal stresses were both nonaxisymmetric.

It is a natural inclination to implement the Fourier method to solve the thermal buckling problems for axisymmetric geometries. The methodology introduced in this research has been adapted from the prior research on TEI problems in brakes and clutches [11] as well as thermoelastic damping in microelectromechanical systems (MEMS) systems [12, 13]. Although the mechanisms differ considerably in these phenomena, the similar strategy to reduce the dimensionality through the Fourier scheme equally applies. For brakes and clutches in particular, due to their ring shapes, the temperature and displacement can be expressed in the Fourier terms and hence the circumferential dependence of the variables can be eliminated from the governing equations. This leads to a finite element formulation only on the cross-sectional area. With the implementation of planar elements, the computational effort can greatly be reduced. However, each node retains all three degrees of freedom along the radial, axial, and circumferential directions, respectively.

Method

According to the theory of elasticity, buckling is caused by the geometric nonlinearity in a deformed structure, which is equivalent to inserting an additional stiffness term to the system. The general finite element formulation of the buckling problem involves the construction of *stress stiffness matrix* $[K_\sigma]$ that is added to the stiffness matrix $[K]$. This stress stiffness matrix is then used to develop an eigenvalue equation for the buckling load as follows [14]:

$$- [K_\sigma]^{-1}[K]\{\delta U\} = \lambda\{\delta U\} \tag{1}$$

in which the eigenvalue λ is the multiplier of the reference load. $\{\delta U\}$ is the buckling displacement, which can be caused by any type of mechanical loadings such as bending moments or thermal stresses.

The stress stiffness matrix is related to the geometric nonlinearity in the Green strains [15]. In general, the Green strain tensor, E, contains both the linear and quadratic terms and is based on the following definition [16]:

$$E = \frac{1}{2}\left(F^{\mathrm{T}} \cdot F - I\right) \tag{2}$$

where I is the identity matrix, and the deformation gradient, F, can be expressed in the cylindrical coordinate systems

$$F = \begin{bmatrix} 1 + \frac{\partial u_{\mathrm{r}}}{\partial r} & \frac{1}{r}\frac{\partial u_{\mathrm{r}}}{\partial \theta} - \frac{u_\theta}{r} & \frac{\partial u_{\mathrm{r}}}{\partial z} \\ \frac{\partial u_\theta}{\partial r} & 1 + \frac{1}{r}\frac{\partial u_\theta}{\partial \theta} + \frac{u_{\mathrm{r}}}{r} & \frac{\partial u_\theta}{\partial z} \\ \frac{\partial u_{\mathrm{z}}}{\partial r} & \frac{1}{r}\frac{\partial u_{\mathrm{z}}}{\partial \theta} & 1 + \frac{\partial u_{\mathrm{z}}}{\partial z} \end{bmatrix} \tag{3}$$

The linear terms of the strains in cylindrical coordinates can be expressed as [17]

$$\varepsilon = \begin{Bmatrix} \varepsilon_{\mathrm{r}} \\ \varepsilon_{\mathrm{z}} \\ \varepsilon_\theta \\ \gamma_{\mathrm{rz}} \\ \gamma_{\mathrm{z}\theta} \\ \gamma_{\theta r} \end{Bmatrix} = \begin{Bmatrix} \frac{\partial u_{\mathrm{r}}}{\partial r} \\ \frac{\partial u_{\mathrm{z}}}{\partial z} \\ \frac{u}{r} + \frac{1}{r}\frac{\partial u_\theta}{\partial \theta} \\ \frac{\partial u_{\mathrm{r}}}{\partial z} + \frac{\partial u_{\mathrm{z}}}{\partial r} \\ \frac{\partial u_\theta}{\partial z} + \frac{1}{r}\frac{\partial u_{\mathrm{z}}}{\partial \theta} \\ \frac{1}{r}\frac{\partial u_{\mathrm{r}}}{\partial \theta} + \frac{\partial u_\theta}{\partial r} - \frac{u_\theta}{r} \end{Bmatrix} \tag{4}$$

where u_r, u_θ, u_z are the displacement components along the radial, circumferential, and the axial direction, respectively. By subtracting the linear terms from the Green strains, we can obtain the following nonlinear terms:

$$\Delta E = \begin{bmatrix} \Delta E_{11} & \Delta E_{12} & \Delta E_{13} \\ \Delta E_{21} & \Delta E_{22} & \Delta E_{23} \\ \Delta E_{31} & \Delta E_{32} & \Delta E_{33} \end{bmatrix} \tag{5}$$

where

$$\Delta E_{11} = \frac{1}{2}\left[\left(\frac{\partial u_r}{\partial r}\right)^2 + \left(\frac{\partial u_\theta}{\partial r}\right)^2 + \left(\frac{\partial u_z}{\partial r}\right)^2\right] \tag{6}$$

$$\Delta E_{12} = \frac{1}{2}\left[-\frac{u_\theta}{r}\frac{\partial u_r}{\partial r} + \frac{u_r}{r}\frac{\partial u_\theta}{\partial r} + \frac{1}{r}\frac{\partial u_r}{\partial \theta}\frac{\partial u_r}{\partial r} + \frac{1}{r}\frac{\partial u_\theta}{\partial r}\frac{\partial u_\theta}{\partial \theta} + \frac{1}{r}\frac{\partial u_z}{\partial r}\frac{\partial u_z}{\partial \theta}\right] \tag{7}$$

$$\Delta E_{13} = \frac{1}{2}\left[\frac{\partial u_r}{\partial r}\frac{\partial u_r}{\partial z} + \frac{\partial u_\theta}{\partial r}\frac{\partial u_\theta}{\partial z} + \frac{\partial u_z}{\partial r}\frac{\partial u_z}{\partial z}\right] \tag{8}$$

$$\Delta E_{22} = \frac{1}{2}\left[\left(\frac{u_\theta}{r}\right)^2 + \left(\frac{u_r}{r}\right)^2 - \frac{2u_\theta}{r^2}\frac{\partial u_r}{\partial \theta} + \frac{2u_r}{r^2}\frac{\partial u_\theta}{\partial \theta} + \frac{1}{r^2}\left(\frac{\partial u_r}{\partial \theta}\right)^2 + \frac{1}{r^2}\left(\frac{\partial u_\theta}{\partial \theta}\right)^2 + \frac{1}{r^2}\left(\frac{\partial u_z}{\partial \theta}\right)^2\right] \tag{9}$$

$$\Delta E_{23} = \frac{1}{2}\left[-\frac{u_\theta}{r}\frac{\partial u_r}{\partial z} + \frac{u_r}{r}\frac{\partial u_\theta}{\partial z} + \frac{1}{r}\frac{\partial u_r}{\partial \theta}\frac{\partial u_r}{\partial z} + \frac{1}{r}\frac{\partial u_\theta}{\partial \theta}\frac{\partial u_\theta}{\partial z} + \frac{1}{r}\frac{\partial u_z}{\partial \theta}\frac{\partial u_z}{\partial z}\right] \tag{10}$$

$$\Delta E_{33} = \frac{1}{2}\left[\left(\frac{\partial u_r}{\partial z}\right)^2 + \left(\frac{\partial u_\theta}{\partial z}\right)^2 + \left(\frac{\partial u_z}{\partial z}\right)^2\right] \tag{11}$$

$$\Delta E_{21} = \Delta E_{12} \tag{12}$$

$$\Delta E_{31} = \Delta E_{13} \tag{13}$$

$$\Delta E_{32} = \Delta E_{23} \tag{14}$$

We assume the periodic distributions of the temperature and displacements as follows:

$$T = \Theta\cos(p\theta); \quad u_r = U_r\cos(n\theta); \quad u_\theta = U_\theta\sin(n\theta); \quad u_z = U_z\cos(n\theta) \tag{15}$$

in which p represents the wave number (i.e., "hot spot" number) of the temperature distribution along the circumference; n represents the wave number of the deformation in the circumference. In general, p is not necessarily equal to n. For example, a circumferentially uniform temperature distribution ($p = 0$) can lead to both *coning* modes ($n = 0$) and *potato chip* modes ($n \neq 0$).

According to [14], the stress stiffness matrix can be obtained through

$$[K_\sigma] = \int [G]^T \begin{bmatrix} s & 0 & 0 \\ 0 & s & 0 \\ 0 & 0 & s \end{bmatrix} [G]\mathrm{d}V \tag{16}$$

in which V represents the volume, G is obtained from the nonlinear terms ΔE in the Green strains and the shape functions $[N]$. The matrix $[s]$ contains the thermal stresses induced by the reference load.

$$[s] = \begin{bmatrix} \sigma_{rr} & \sigma_{r\theta} & \sigma_{zr} \\ \sigma_{r\theta} & \sigma_{\theta\theta} & \sigma_{\theta z} \\ \sigma_{zr} & \sigma_{\theta z} & \sigma_{zz} \end{bmatrix} \tag{17}$$

The constitutive law of thermoelasticity has the following matrix form

$$\sigma = [C]\varepsilon - [D]T \tag{18}$$

where the coefficient matrix C is the stress–strain relationship.

$$[C] = \frac{E}{(1+v)(1-2v)} \begin{bmatrix} 1-v & v & v & 0 & 0 & 0 \\ v & 1-v & v & 0 & 0 & 0 \\ v & v & 1-v & 0 & 0 & 0 \\ 0 & 0 & 0 & 1-2v & 0 & 0 \\ 0 & 0 & 0 & 0 & 1-2v & 0 \\ 0 & 0 & 0 & 0 & 0 & 1-2v \end{bmatrix} \tag{19}$$

where E is Young's modulus and v is Poisson's ratio. D is associated with thermal expansions

$$[D] = \frac{E\alpha}{(1-2v)} \begin{bmatrix} 1 & 1 & 1 & 0 & 0 & 0 \end{bmatrix}^{\mathrm{T}} \tag{20}$$

The strain vector ϵ can be expressed in a matrix form related to the nodal displacement vector U:

$$\varepsilon = [B]U \tag{21}$$

where

$$[B] = \begin{bmatrix} B_1 & B_2 & B_3 & B_4 \end{bmatrix} \tag{22}$$

$$[B_i] = \begin{bmatrix} \frac{\partial N_i}{\partial r} & 0 & 0 \\ \frac{N_i}{r} & \frac{nN_i}{r} & 0 \\ 0 & 0 & \frac{\partial N_i}{\partial z} \\ -\frac{nN_i}{2r} & \frac{1}{2}\left(\frac{\partial N_i}{\partial r} - \frac{N_i}{r}\right) & 0 \\ 0 & \frac{1}{2}\frac{\partial N_i}{\partial z} & -\frac{nN_i}{2r} \\ \frac{1}{2}\frac{\partial N_i}{\partial z} & 0 & \frac{1}{2}\frac{\partial N_i}{\partial r} \end{bmatrix} \quad (i = 1, 2, 3, 4) \tag{23}$$

Note that σ and ϵ here are thermally induced stresses and strains. Since T varies with $\cos(p\theta)$, apparently σ also varies with $\cos(p\theta)$. It implies that the nonlinear terms in the Green strains ΔE would be zero if both n and p are nonzero integers, which leads to a zero stress stiffness matrix, due to the following orthogonality relationships of the sine and cosine functions:

$$\int_0^{2\pi} \cos^2(n\theta)\cos(p\theta)d\theta = 0$$
$$\int_0^{2\pi} \sin^2(n\theta)\cos(p\theta)d\theta = 0 \tag{24}$$
$$\int_0^{2\pi} \cos(n\theta)\sin(n\theta)\cos(p\theta)d\theta = 0$$

For an axisymmetric temperature distribution, namely, $p = 0$, the above formulation leads to

$$[K_\sigma]^{\{r\}} = \iint \begin{bmatrix} \sigma_{\mathrm{rr}}\frac{\partial[N]}{\partial r}\frac{\partial[N]^{\mathrm{T}}}{\partial r} + \sigma_{\theta\theta}\frac{(n^2+1)}{r^2}[N][N]^{\mathrm{T}} + \sigma_{\mathrm{zz}}\frac{\partial[N]}{\partial r}\frac{\partial[N]^{\mathrm{T}}}{\partial r} + \\ \sigma_{\mathrm{rz}}\left(\frac{\partial[N]}{\partial r}\frac{\partial[N]^{\mathrm{T}}}{\partial z} + \frac{\partial[N]}{\partial z}\frac{\partial[N]^{\mathrm{T}}}{\partial r}\right) \end{bmatrix} r\,dr\,dz \tag{25}$$

$$[K_\sigma]^{\{\theta\}} = [K_\sigma]^{\{r\}} \tag{26}$$

$$[K_\sigma]^{\{z\}} = \iint \begin{bmatrix} \sigma_{\mathrm{rr}}\frac{\partial[N]}{\partial r}\frac{\partial[N]^{\mathrm{T}}}{\partial r} + \sigma_{\theta\theta}\frac{n^2}{r^2}[N][N]^{\mathrm{T}} + \sigma_{\mathrm{zz}}\frac{\partial[N]}{\partial r}\frac{\partial[N]^{\mathrm{T}}}{\partial r} + \\ \sigma_{\mathrm{rz}}\left(\frac{\partial[N]}{\partial r}\frac{\partial[N]^{\mathrm{T}}}{\partial z} + \frac{\partial[N]}{\partial z}\frac{\partial[N]^{\mathrm{T}}}{\partial r}\right) \end{bmatrix} r\,dr\,dz \tag{27}$$

In a special case where both temperature and deformation are axisymmetric, i.e., $n = p = 0$ and $U_\theta = 0$, the above equations can further be reduced to

$$[K_\sigma]^{\{r\}} = \iint \left[\begin{array}{l} \sigma_{rr} \frac{\partial [N]}{\partial r} \frac{\partial [N]^T}{\partial r} + \sigma_{\theta\theta} \frac{1}{r^2} [N][N]^T + \sigma_{zz} \frac{\partial [N]}{\partial r} \frac{\partial [N]^T}{\partial r} + \\ \sigma_{rz} \left(\frac{\partial [N]}{\partial r} \frac{\partial [N]^T}{\partial z} + \frac{\partial [N]}{\partial z} \frac{\partial [N]^T}{\partial r} \right) \end{array} \right] r dr dz \tag{28}$$

$$[K_\sigma]^{\{z\}} = \iint \left[\sigma_{rr} \frac{\partial [N]}{\partial r} \frac{\partial [N]^T}{\partial r} + \sigma_{zz} \frac{\partial [N]}{\partial r} \frac{\partial [N]^T}{\partial r} + \sigma_{rz} \left(\frac{\partial [N]}{\partial r} \frac{\partial [N]^T}{\partial z} + \frac{\partial [N]}{\partial z} \frac{\partial [N]^T}{\partial r} \right) \right] r dr dz \tag{29}$$

The stiffness matrix $[K]$ can be obtained using the finite element formulation discussed in the prior research [11]:

$$[K_e] = \iint_\Omega [B]^T [C][B] r dr dz \tag{30}$$

The above finite element method based on the Fourier scheme has successfully been converted into a Matlab code. The eigenvalue equation, Eq. (1), is solved to find the buckling temperature gradient by implementing the built-in eigenvalue function *eig* in Matlab.

Results and discussion

Convergence study

To validate the proposed Fourier method, we first performed a convergence test on the critical buckling temperature of an annular ring with free boundaries. The material properties and dimensions of the ring are tabulated in Table 1. The axisymmetric mode shape has been assumed, so that the circumferential wave number is set to zero in the analysis. The axisymmetric elements with the linear interpolating functions have been used to discretize the cross-sectional area of the ring. The temperature is assumed as a linear function of the radial coordinate with a zero value at the inner radius and the maximum value at the outer radius. Therefore the eigenvalue, or the buckling temperature, is equivalent to the temperature at the outer radius. A positive eigenvalue indicates an increase in the temperature in the radius, whereas a negative one indicates a decrease in the temperature. Figure 1 shows the four dominant buckling mode shapes from the finite element analysis. These modes have the lowest buckling temperatures among all modes. The colors in Figure 1 demonstrate the distribution of the magnitude of the nodal displacement. The element number along the thickness is set to five, whereas the element number in the radius, m, varies between 5 and 100 to show the relationship between the buckling temperature and the mesh size (Figure 2). The results of the three leading modes are also compared. The first mode is a coning mode, with the axial displacement linearly distributed in the radius. The computed buckling temperature based on the Fourier model starts with -185.9 at $m = 5$ and converges to -178.3 at $m = 100$, with a variation of merely 4%, showing an excellent convergence speed for the first mode. The negative value indicates that the temperature distribution is actually reversed, i.e., the higher temperature occurs at the inner radius. The result was also compared with Abaqus using the axisymmetric element type CAX4I, which yielded a buckling temperature of -177.0 at $m = 100$. For higher order modes, the deformed mode patterns (i.e., the eigenvectors) have nonlinear profiles, with one or multiple reversals across the radius. The computed buckling temperature converges well when m is above 50 but deviates significantly when m falls below 20. In addition, the results based on the Fourier model agree well with the results from Abaqus when $m = 100$. It has been concluded that 50 elements in the radial direction are sufficient to obtain a satisfactory numerical accuracy. It is noticed that the second and third modes have significantly higher buckling temperatures with two or three orders of magnitude higher than the first mode. In practice, typical operating temperatures of brakes or clutches are well below 1000°C, therefore we conclude that the coning mode is the only axisymmetric mode having practical significance in engineering applications.

Table 1. Parameters used in the thermal buckling models.

Inner radius R_i (mm)	Outer radius R_o (mm)	Thickness a (mm)	Young's modulus E (GPa)	Poisson's ratio ν	Thermal expansion coefficient α (K^{-1})
86	125	3	160	0.29	1.27×10^{-5}
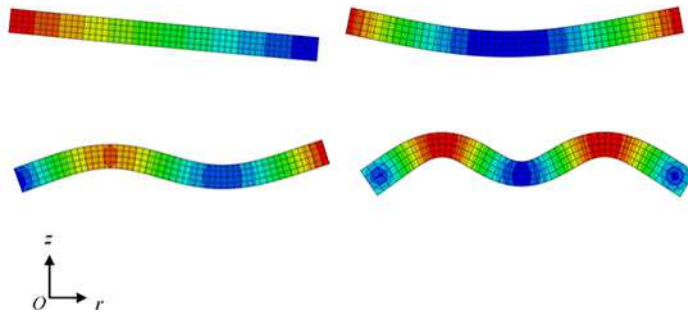
Figure 1. The dominant four axisymmetric buckling modes for an annular ring with free boundaries.
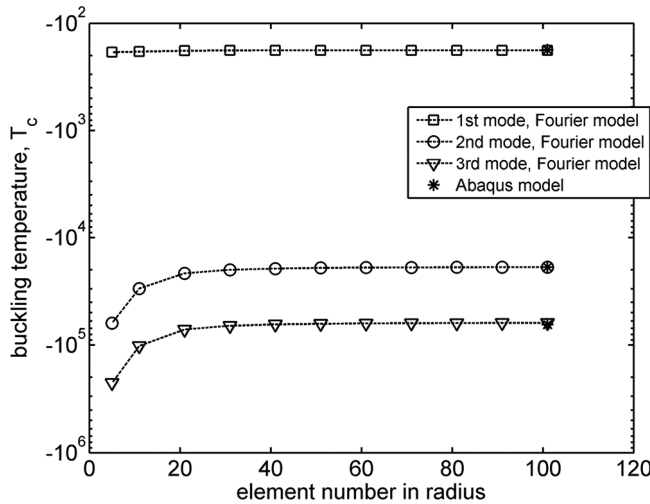
Figure 2. A convergence study on the relationship between the buckling temperature and the element number in the radial direction.

Effects of boundary conditions

It is well known that an elastic column under different boundary conditions has different buckling loads. The boundary condition in the current problem plays an equally important role in the buckling behavior. Figure 3 is the relationship between the buckling temperature and the buckling mode using the Fourier model and Abaqus, for a clutch model with free boundaries. Fifty elements were used in the radius for all results. For the first three dominant modes, the two results are almost identical. Starting from the fourth mode, however, there is an apparent discrepancy between the two curves. This is possibly caused by the different interpolating functions and the integration schemes involved in the two methods. Also, shear locking may play an important role since the linear elements have been used in the Matlab computation.

Figure 4 shows the leading buckling modes for a clutch model with fixed boundaries at the inner radius. The first model looks like a cantilever beam despite the fact that it represents the cross section of an annular ring. The relationship between the buckling temperature and the buckling mode for the model with fixed boundary conditions at the inner radius is shown in Figure 5. Again, the results of the first three modes show good agreements, but they deviate each other starting from the fourth mode. In
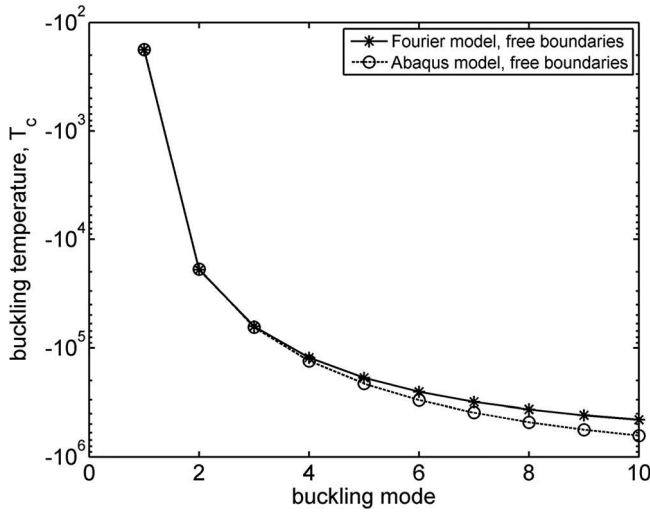
Figure 3. Comparison of the computed buckling temperature between the Fourier model and Abaqus for an annular ring with free boundaries.
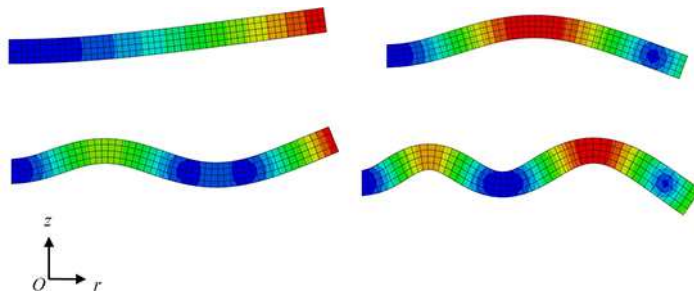
Figure 4. The dominant four axisymmetric buckling modes for an annular ring with fixed inner radius.
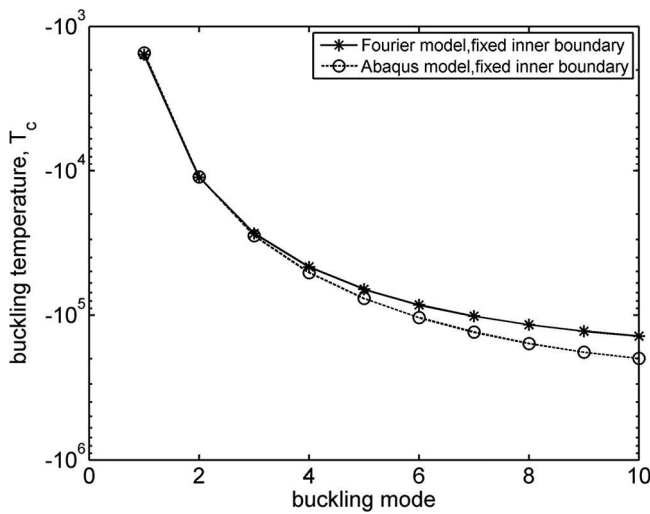
Figure 5. Comparison of the computed buckling temperature between the Fourier model and Abaqus for an annular ring with fixed inner radius.

fact there is a discrepancy of 10% for the fourth mode. In the model with fixed boundaries, however, the buckling temperatures are much higher than those of the model with free boundaries. For example, the critical temperature of the first mode here is -1570, with an order of magnitude higher than the value of -178 for free boundaries.

Nonaxisymmetric buckling modes

In the above discussions on axisymmetric buckling modes, we found that the buckling temperatures are typically much higher than the operating temperatures in real clutch applications, and they only have theoretical significance except for the first mode or the coning mode. In comparison, nonaxisymmetric buckling modes have much lower critical temperatures and they are therefore of more significant importance. We investigated these nonaxisymmetric modes with the implementation of the Fourier elements by setting the circumferential wave number to a nonzero integer in the finite element formulation. The temperature distribution is still assumed to be axisymmetric, even though the deformed shape has multiple waves in the circumference. We encountered some numerical difficulties, when implementing the model with free boundaries due to the singularities in the matrices. To simplify the mathematical treatment, the fixed boundary condition is assumed at the inner radius here to prevent rigid body motions in the eigenmodes. The results from both the Fourier method and Abaqus have been obtained for comparison. In the Fourier model, the cross section has been discretized in the same way as the previous discussions on the axisymmetric modes. In Abaqus, the element type C3D8I (i.e., linear hexahedron 3D elements with incompatible modes to improve the bending behavior) has been used in the computation. The model was discretized in the entire ring with 20 elements along the radius, a single element along the thickness and 100 elements along the circumference. Therefore, the total element number in the 3D finite element model is 2000. The first 100 eigenmodes were extracted to investigate the relationship between the buckling temperatures and the circumferential wave number.

Figure 6 shows the dominant mode shapes. Mode A is the axisymmetric coning mode with $n = 0$, which is identical to the first mode in Figure 4. Modes B–F are nonaxisymmetric buckling modes with n being a nonzero integer. Among them, Mode D with $n = 6$ is the dominant mode with the lowest critical buckling temperature of 746 based on the Fourier model. Figure 7 shows the relationship between the critical temperature and the circumferential wave number. Clearly, the Fourier model and the Abaqus model yielded very close results over the entire range of wave number from 0 to 15. The coning mode has the lowest buckling temperature (absolute value) among the three modes with the negative eigenvalues. There is an interesting transition on the sign of the buckling temperature from negative at $n = 2$ to positive at $n = 3$. Moreover, the buckling temperature has a nonlinear relationship with n in the positive region, with the lowest value located at $n = 6$ as mentioned above. Figure 8 is the same as Figure 7, except that the positive region has been enlarged. This figure is reminiscent of the relationship between the critical sliding speed and the wave number in TEI analysis in which there exists a lowest sliding speed. It is noticed that the modes with $n = 5$–9 have critical temperatures below 1000°C, which could be in the vicinity of the temperature range in clutches. In real applications, the mechanical constrains such as the teeth on the edge of clutch disk or the splines in the shaft may impose restrictions on the available mode patterns. Therefore, any of these modes could be excited depending on the specific boundary conditions.

It should be pointed out that the above results were based on the boundary condition with fixed inner radius, which is a rare case in realistic applications. Some of the buckling temperatures obtained are higher than the melting points of metals and these modes can never be available in reality. For a model with free boundaries, on the other hand, the dominant mode is most likely a coning mode with the corresponding buckling temperature much lower than the value aforementioned [9]. In real applications, the boundary conditions of the discs are somewhere between fully constrained and freely movable. As a consequence, the realistic buckling temperature should be interpolated between two extremes. We
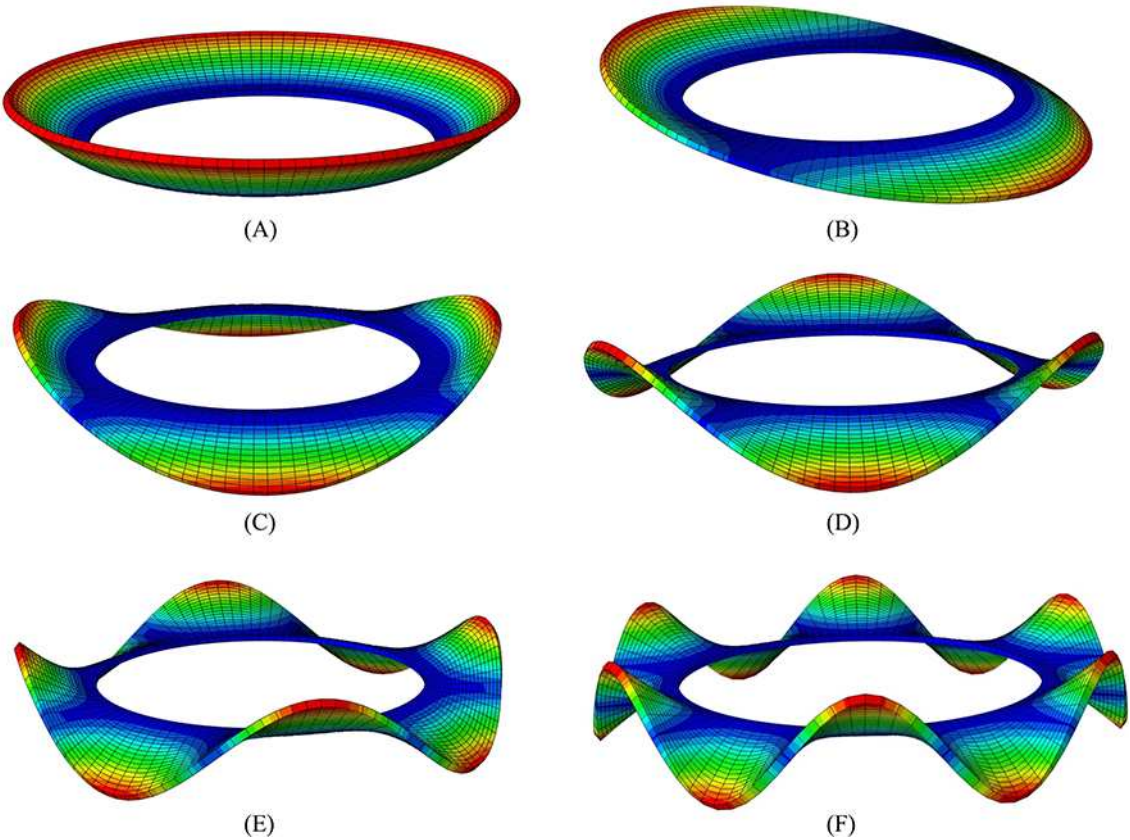
Figure 6. Dominant buckling modes for an annular ring with fixed inner radius, with both axisymmetric and nonaxisymmetric modes included.
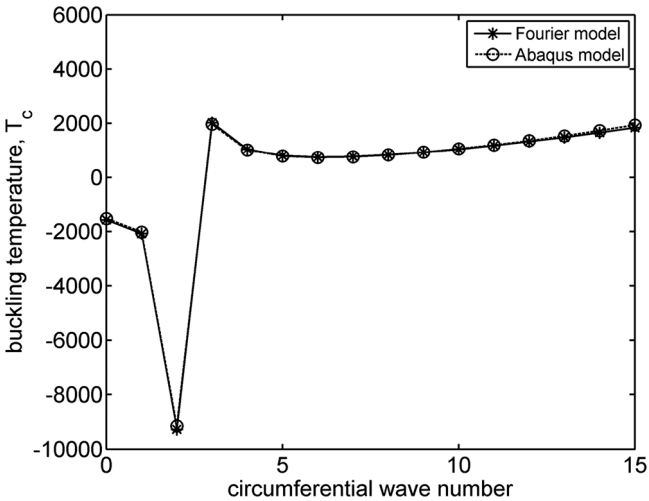
Figure 7. Buckling temperature as a function of circumferential wave number for an annular ring with fixed inner radius.

encountered some numerical difficulties when implementing the free boundary conditions to the Fourier model for nonaxisymmetric buckling modes, due to the singularities caused by a freely movable rigid body. We will endeavor to resolve this issue in the future.
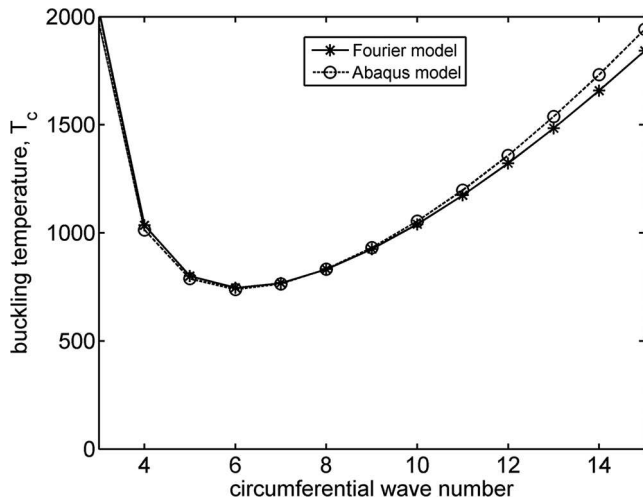
Figure 8. Enlarged figure showing the positive buckling temperature as a function of circumferential wave number.

Conclusion

A reduced finite element method using the Fourier scheme is developed to predict the critical thermal buckling temperature and the associated deformation modes in automotive brakes and clutches or any other ring-shaped mechanical components subjected to high thermal stresses. In this study, the temperature distribution is a predefined field, and the matrix equation is constructed based on the Green strain formulation with geometric nonlinearities. The reduced dimensionality in the finite element discretization greatly improved the computational efficiency. The numerical solutions obtained from the Fourier scheme agree with those from Abaqus using a full three-dimensional model. Both wavy modes and coning modes have been obtained from the eigenvectors of the governing equation. The results have shown the existence of the lowest buckling temperature among all mode shapes. The circumferential wave number at the global lowest buckling temperature varies and it is determined by the material properties and geometric shapes. The buckling temperature of the model with free boundaries is significantly lower than the one with constrained boundaries. Although the analyses were based on a linear radial temperature assumption (which was consistent with the multidisc clutch experiment recently reported in the literature), the same methodology can be applied to other applications involving nonlinear temperature profiles as well. In addition, although the traditional TEI analysis does not incorporate the geometric nonlinearity, the current research implies that both thermal buckling and TEI exhibit similar mode patterns and that the two phenomena could be coupled together as the temperature gradient is sufficiently high.

References

1. A. E. Anderson and R. A. Knapp, Hot Spotting in Automotive Friction Systems, *Wear*, vol. 135, pp. 319–337, 1990.
2. T. K. Kao, J. W. Richmond, and A. Douarre, Brake Disc Hot Spotting and Thermal Judder: An Experimental and Finite Element Study, *Int. J. Vehicle Design*, vol. 23, pp. 276–296, 2000.
3. S. Panier, P. Dufrenoy, and D. Weichert, An Experimental Investigation of Hot Spots in Railway Disc Brakes, *Wear*, vol. 256, pp. 764–773, 2004.
4. C. Xiong, B. Ma, H. Li, F. Zhang, and D. Wu, Experimental Study and Thermal Analysis on the Buckling of Friction Components in Multi-Disc Clutch, *J. Thermal Stresses*, vol. 38, pp. 1325–1345, 2015.
5. P. Zagrodzki, Numerical Analysis of Temperature Fields and Thermal Stresses in the Friction Discs of a Multidisc Wet Clutch, *Wear*, vol. 101, pp. 255–271, 1985.
6. N. Audebert, J. R. Barber, and P. Zagrodzki, Buckling of Automatic Transmission Clutch Plates due to Thermoelastic/Plastic Residual Stresses, *J. Thermal Stresses*, vol. 21, pp. 309–326, 1998.

7. S. P. Timoshenko and J. M. Gere, *Theory of Elastic Stability*, 2nd edn, Dover Publications, New York, 1961.
8. C. Ma, Thermal Buckling of Automotive Brake Discs, Ph.D. dissertation, University of Michigan, Ann Arbor, 2004.
9. J. Zhao, Z. Chen, H. Yang, and Y.B. Yi, Finite Element Analysis of Thermal Buckling in Automotive Clutch Plates, *J. Thermal Stresses*, vol. 39, pp. 77–89, 2016.
10. Abaqus Software User's Manual 6.9, Providence, RI, 2009.
11. Y. B. Yi, J. R. Barber, and P. Zagrodzki, Eigenvalue Solution of Thermoelastic Instability Problems Using Fourier Reduction, *Proc. R. Soc. Lon. A*, vol. 456, pp. 2799–2821, 2003.
12. Y. B. Yi and M. A. Matin, Eigenvalue Solution of Thermoelastic Damping in Beam Resonators Using a Finite Element Analysis, *J. Vib. Acoust.*, vol. 129, pp. 478–483, 2007.
13. Y. B. Yi, Geometric Effects on Thermoelastic Damping in MEMS Resonators, *J. Sound Vib.*, vol. 309, pp. 588–599, 2008.
14. R. D. Cook, D. S. Malkus, M. E. Plesha, and R. J. Witt, *Concepts and Applications of Finite Element Analysis*, 4th ed., John Wiley & Sons, Hoboken, New Jersey, 2002.
15. L. E. Malvern, *Introduction to the Mechanics of a Continuous Medium*, Prentice-Hall, Englewood Cliffs, New Jersey, 1969.
16. E. N. Dvorkin and M. B. Goldschmit, *Nonlinear Continua*, Springer, Berlin, Germany, 2005.
17. O. C. Zienkiewicz and R. L. Taylor, *The Finite Element Method*, 5th ed., Butterworth-Heinemann, Oxford, 2000.